Check for updates

Wiley
Journal of Sensors
Volume 2025, Article ID 9990501, 12 pages
https://doi.org/10.1155/js/9990501

WILEY

Research Article

Evaluation of Caffeine Content in Carbonated and Energy Drinks Using a Sensor-Modified Polyaniline–Silver Nanoparticles

Charlton van der Horst,[1] **Shaheeda Adonis**,[1] **Eric Gil**,[2] **and Vernon Somerset**[1]

[1]*Department of Chemistry, Faculty of Applied Sciences, Cape Peninsula University of Technology, Bellville Campus, Bellville, Western Cape, South Africa*
[2]*Faculdade de Farmácia, Universidade Federal de Goiás, Campus Colemar Natal e Silva, Praça Universitára, CEP: 74605-220, Goiânia, Goiâs, Brazil*

Correspondence should be addressed to Vernon Somerset; somersetv@cput.ac.za

Received 13 September 2024; Revised 2 September 2025; Accepted 9 September 2025

Academic Editor: Bruno C. Janegitz

Copyright © 2025 Charlton van der Horst et al. Journal of Sensors published by John Wiley & Sons Ltd. This is an open access article under the terms of the Creative Commons Attribution License, which permits use, distribution and reproduction in any medium, provided the original work is properly cited.

The detection of caffeine (CAF) is essential due to its widespread use and potential health impacts, including effects on sleep and anxiety. In this study, polyaniline (PANI) and PANI doped with silver nanoparticles (AgNPs) were synthesized to effectively detect CAF in beverage samples. The chemically synthesized polymers were characterized using transmission electron microscopy (TEM), scanning electron microscopy (SEM), and electrochemical impedance spectroscopy (EIS) to investigate their morphological and electrochemical properties. Differential pulse voltammetry (DPV) and cyclic voltammetry (CV) were employed to determine CAF concentrations in caffeinated beverages. SEM results revealed that PANI and PANI–Ag films are spherical, with an average diameter of ~100 nm, while TEM analysis showed AgNPs within the PANI–Ag matrix had an average particle size of 5–10 nm. Optimized experimental conditions yielded a linear response for CAF concentrations ranging from 10 to 90 μM, with an R^2 value of 0.9935. The detection limit for the PANI–Ag electrochemical sensor was determined to be 0.38 μM ($n = 3$). This sensor is important for monitoring CAF levels in beverages, contributing to public health awareness and safety, with electrochemical analysis aligning well with labeled values.

Keywords: beverage samples; caffeine; differential pulse voltammetry; polyaniline; silver nanoparticles

1. Introduction

A natural stimulant such as caffeine (CAF) or 1,3,7-trimethylxantine is most found in cacao plants, coffee, numerous drugs, kola nuts, and tea leaves [1]. CAF is found naturally in consumed foods or added to cola-type soft drinks and energy drinks. Due to its psychoactive effects, such as diuresis, central nervous system stimulation, and gastric acid secretion, CAF is also used in many pharmaceutical formulations [2–4]. Nowadays, numerous analytical methods are used in determining CAF, such as liquid chromatography with photodiode array [5, 6], gas chromatography [7–9], UV–Vis [10], FT-IR [11–13], and NMR [14]. Disadvantages such as the expense of the method, sample pretreatment, and time-consuming are associated with these methods. Then there are also derivatization, preconcentration, and highly trained personnel, which are also disadvantages of these methods. In the electrochemical analysis of CAF, many modifiers have been utilized to modify clean, glassy carbon (C) electrodes (GCEs) and to improve their analytical performance. The electro-active modifiers used are bimetallic nanoparticles (NPs) [15, 16], metal oxides [15, 16], C nanotubes [17, 18], redox polymers [19, 20], clay materials [21, 22], and graphene [23, 24].

Conducting polymers (CPs) have received increasing attention over the past years due to their formation and characterization and are widely employed in many applications of sensors, batteries, and microelectronic devices. The application of CPs as active layers in electrochemical sensors has also

received increased attention since there is evidence that organic vapors and adsorbed gas molecules can cause a transformation in electrical conductivity in the polymer matrix. The synthesis of CPs can be done in the presence of a given counter ion by electrochemical deposition, which allows film preparation at a well-defined redox potential. The counter ion also defines the characteristics and level of the doping reaction. The formation of the polymer film is directly on a metal (or transducer) surface through electropolymerization using the appropriate monomers in the presence of an oxidant. These have enabled researchers to study several polymers' chemical and physical properties (i.e., morphology, catalytic activity, stability, structure, and conductivity), tailoring the polymers to specific sensor applications [25–27].

In this study, the focus has been on polyaniline (PANI) and silver NPs (AgNPs). PANI is one of the essential CPs, and it exists in three cathodic states. The three oxidation states of PANI are emeraldine (the stable intermediate form), pernigraniline (the oxidized form), and leucoemeraldine (the reduced form). Pernigraniline and emeraldine bases may react with acids to form their corresponding salts [28]. PANI is the most promising CP among all the others due to its low cost of monomer, good environmental stability, and controllable electrical properties [29]. The electrical properties of PANI can be reversibly controlled by protonation and charge transfer doping. It is a potential material for actuators, microelectronic devices, and chemical and biological sensors [30–33].

In recent developments in nanoscience and nanotechnology, the roles of CPs are also critical. Various methods have synthesized CPs, such as electrospinning, template synthesis, and scanning probe electrochemical polymerization. These methods can synthesize polymers into nanostructures (e.g., nanorods, nanofibers, and nanotubes) [34]. Three synthesis methods can generally prepare the synthesis of noble metals with PANI. The first method involves the synthesis of PANI in the presence of metal NPs, the second method involves noble-metal salts or acids using PANI as the reductant, and the third method involves noble-metal compounds oxidizing aniline (ANI). Ag metal has recently received significant attention in this respect. The first method has been done by modifying AgNPs with PANI or substituting PANI [35–37].

In the current investigation, the chemical polymerization method successfully synthesized the homopolymer of PANI with the incorporation of AgNPs into the polymer. After synthesizing the PANI and PANI–Ag materials, studies of the electrochemical behavior of the materials were performed using electrochemical impedance spectroscopy (EIS) and cyclic voltammetry (CV). Scanning electron microscopy (SEM) and transmission electron microscopy (TEM) were employed to investigate the morphology of the PANI and PANI–Ag materials. In the literature, it is the first time the PANI–Ag sensor was employed to detect CAF. To assess the suitability of the developed PANI–Ag sensor as an alternative sensor to detect CAF in beverage samples. The constructed PANI–Ag sensor illustrates good electrochemical activity for CAF with a low detection limit and a broad linear range. This procedure is sensitive, simple, fast, and efficient compared to other electrochemical methods.

2. Materials and Methods

2.1. Materials and Reagents. Sulfuric acid (95%), hydrochloric acid (37%), ethanol (absolute 99.9%), and nitric acid (55%) were procured from Merck (South Africa). Ammonium peroxydisulfate (APS) (98%), Ag nitrate, and acetone were purchased from Sigma–Aldrich (Germany). The reagents ANI (99%) and *N*,*N*-dimethylformamide (98%) were also procured from Merck (South Africa). CAF was procured from Sigma–Aldrich (South Africa). We prepared all buffers and stock solutions using Milli-*Q* (Millipore) water.

2.2. Instrumentation. Electrochemical investigations were performed with an Epsilon electrochemical analyzer (BASi Instruments, 2701 Kent Ave., West Lafayette, IN 47906, USA) using CV and differential pulse voltammetry (DPV) modes. The use of a conventional three-electrode system, consisting of a platinum wire auxiliary electrode, a 3.0 M KCl-type Ag/AgCl reference electrode, and a 1.2 mm in diameter platinum disc working electrode, supplied by BASi [38]. A single-compartment electrochemical cell was utilized for all electrochemical analysis at ambient temperatures ($20 \pm 1°C$). A Zahner IM6ex instrument (Germany) was employed for EIS experiments. For optimal sensitivity, the SEM analysis was executed on an LEO 1525 field emission scanning electron microscope with interchangeable accelerating voltages (maximum of 15 kV) [32, 33, 39]. A JEOL 1200-EX II transmission electron microscope was employed for TEM analysis. TEM imaging using conditions of 120 kV, an objective aperture setting of 150 μm, and a spot size of 3 was used. The dried PANI and PANI–Ag samples were dispersed in DMF, sonicated for 5 min, and cast onto a copper grid for measurement [40]. A MegaView camera with Gatan microscopic software was used to image the samples with digital imaging acquisition, with the most effective resolution of 1376×1032 and an exposure time of 2 s.

2.3. Preparation of Materials

2.3.1. Chemical Polymerization of PANI Polymer. The monomer ANI was added to an oxidizing agent, APS. About 200 mL of Milli-*Q* water and concentrated HCl (~1 M) (20 mL) were mixed in a beaker and stirred using a magnetic stirrer. The APS (7.6 g) was added slowly to the above solution and stirred for 5 min. A 3.1 mL of ANI (~0.15 M) was transferred to that solution and stirred for 2 h employing a magnetic stirrer at ambient temperature. After 30 min, a solution with a deep green color was obtained, filtered at the end of the synthesis, cleaned with acetone and Milli-*Q* water, and dried overnight in a fume hood at ambient temperature. The dried polymer was then collected from the paper, milled then transferred to a clean poly top container and stored for further characterization [41, 42].

2.3.2. Chemical Polymerization of PANI–Ag Nanocomposites. The chemical synthesis of a PANI–Ag composite was performed using a similar procedure to that for PANI. After 30 min of stirring, an Ag nitrate solution was added to the PANI solution and stirred for 2 h at ambient temperature.

9161, 2025, 1, Downloaded from https://onlinelibrary.wiley.com/doi/10.1155/js/9990501 by South African Medical Research Council, Wiley Online Library on [27/10/2026]. See the Terms and Conditions (https://onlinelibrary.wiley.com/terms-and-conditions) on Wiley Online Library for rules of use; OA articles are governed by the applicable Creative Commons License

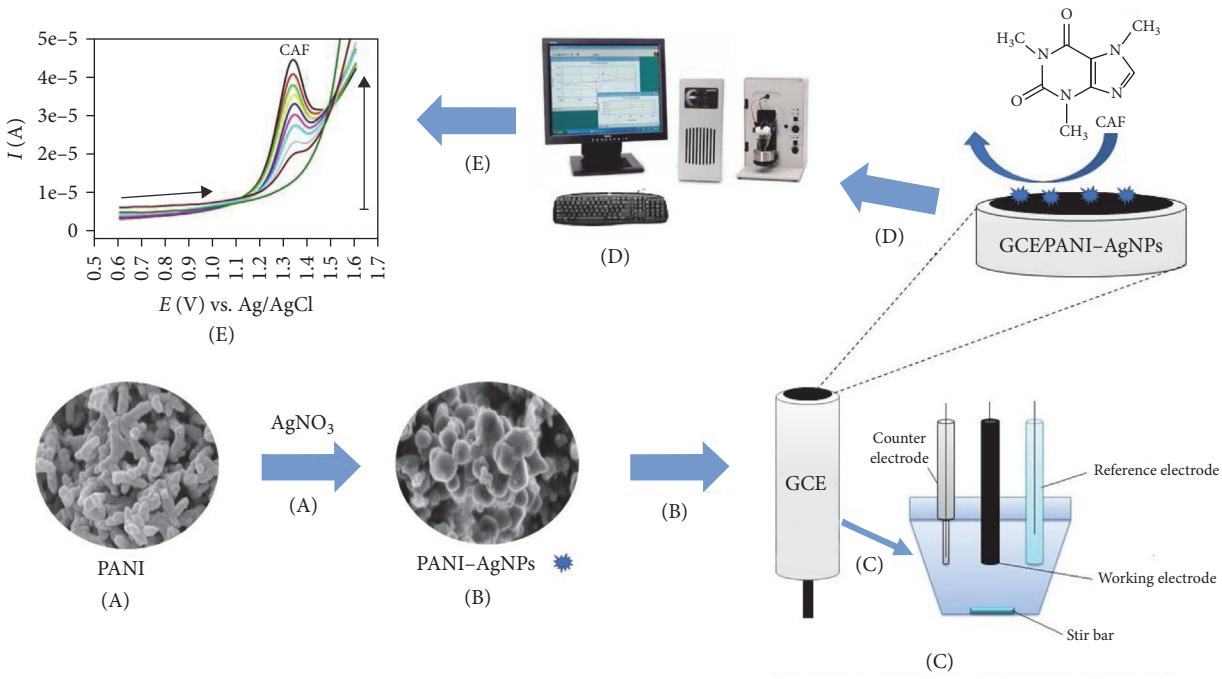

FIGURE 1: Summary of the PANI–Ag/GCE construction and the electrochemical cell setup for the determination of CAF. (A) PANI reacts with $AgNO_3$. (B) PANI–AgNPs drop-coated onto GCE. (C) Three-electrode electrochemical cell. (D) BASI with three-electrode electrochemical cell. (E) Signal processing.

Known concentrations of Ag nitrate (e.g., 0.5 M) were investigated. The resulting polymer nanocomposite was filtered with filter paper, cleaned with acetone, washed with Milli-Q water, and dried overnight at ambient temperature in a fume hood. The resulting polymer nanocomposite was milled, then transferred to a clean poly top container and stored for further characterization [41, 43].

2.3.3. Sensor Preparation. The GCEs were cleaned by polishing followed by an ultrasound bath. Polishing was carried out until a mirrored surface was obtained in a polishing machine with sandpaper made of silicon carbide and an aqueous suspension of 0.5 μm alumina. After sonification, the electrodes were put in ethanol and in an ultrasound bath for 2 min, and then in ultrapure water for another 5 min. After the polished GCE, the cleaned and dried electrodes were dried at room temperature. A small amount of the PANI–Ag suspension to be studied (PANI–AgNPs) was added. The suspension PANI–AgNPs was dried at room temperature, and the constructed sensor was taken to the electrochemical cell to perform electrochemical studies. Figure 1 illustrates the synthesis process of PANI–AgNPs, the modification of GCE with the PANI–Ag nanocomposite, and the three-electrode electrochemical cell used in this study.

3. Results and Discussion

3.1. Microscopy Characterization

3.1.1. SEM Characterization of Polymers. The synthesis conditions were used to prepare PANI to determine the resulting polymers' morphology and structure [44, 45]. SEM is a robust surface physical characterization technique used to study the morphology and structures of both PANI and PANI–Ag nanocomposites. Figure 2 reveals the results of the SEM analysis of the chemically synthesized PANI and PANI–Ag nanocomposite. The results in Figure 2A for the particles of chemically synthesized PANI clearly show the tubular-like nature of the composite obtained, which was found to be evident. The particles in Figure 2A have a diameter between 200 and 500 nm [46, 47].

SEM also determined the morphology and structure of the PANI–Ag (0.5 M) nanocomposites. Figure 2B presents the SEM analysis of the chemically synthesized PANI–Ag nanocomposite at a concentration of 0.5 M. The results in Figure 2B clearly demonstrate that the PANI–Ag nanocomposite particles are spherical and in the nano range, with the incorporation of AgNPs enhancing this morphology. The average particle size of the PANI–Ag nanocomposite is ~100 nm, featuring smaller Ag particles interspersed throughout [48].

3.1.2. TEM. A TEM studied the particle size of the PANI–Ag (0.5 M) polymeric composite. Figure 3 showcases the TEM image results of chemically synthesized PANI–Ag with an Ag concentration of 0.5 M. The AgNPs obtained in this image appear relatively uniform in size and clusters. This TEM image confirms that the polymer for the PANI–Ag nanocomposite in the background is spherical. The average particle size of these AgNPs is between 5 and 10 nm. The EDX spectrum of this PANI–Ag (not shown) exhibits the presence of sulfur (S), oxygen (O), C, Ag, and chlorine (Cl) elements. The EDX spectrum showcases a very high content of the Ag element in the chemically synthesized nanocomposite and indicates that the sample is relatively pure (The EDX results are shown in Supporting Information 1: Figure S1). The sample's appearance of S and Cl

9161, 2025, 1, Downloaded from https://onlinelibrary.wiley.com/doi/10.1155/js/9990501 by South African Medical Research Council, Wiley Online Library on [27/10/2026]. See the Terms and Conditions (https://onlinelibrary.wiley.com/terms-and-conditions) on Wiley Online Library for rules of use; OA articles are governed by the applicable Creative Commons License

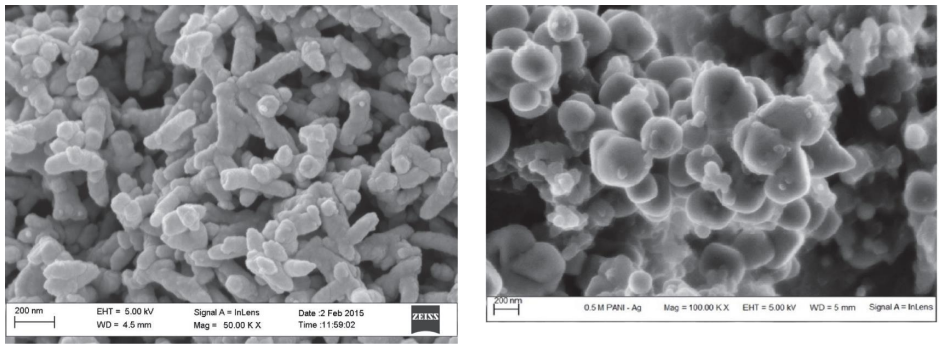

(A) (B)

FIGURE 2: SEM images of chemically synthesized (A) PANI and (B) PANI–Ag polymeric composites.

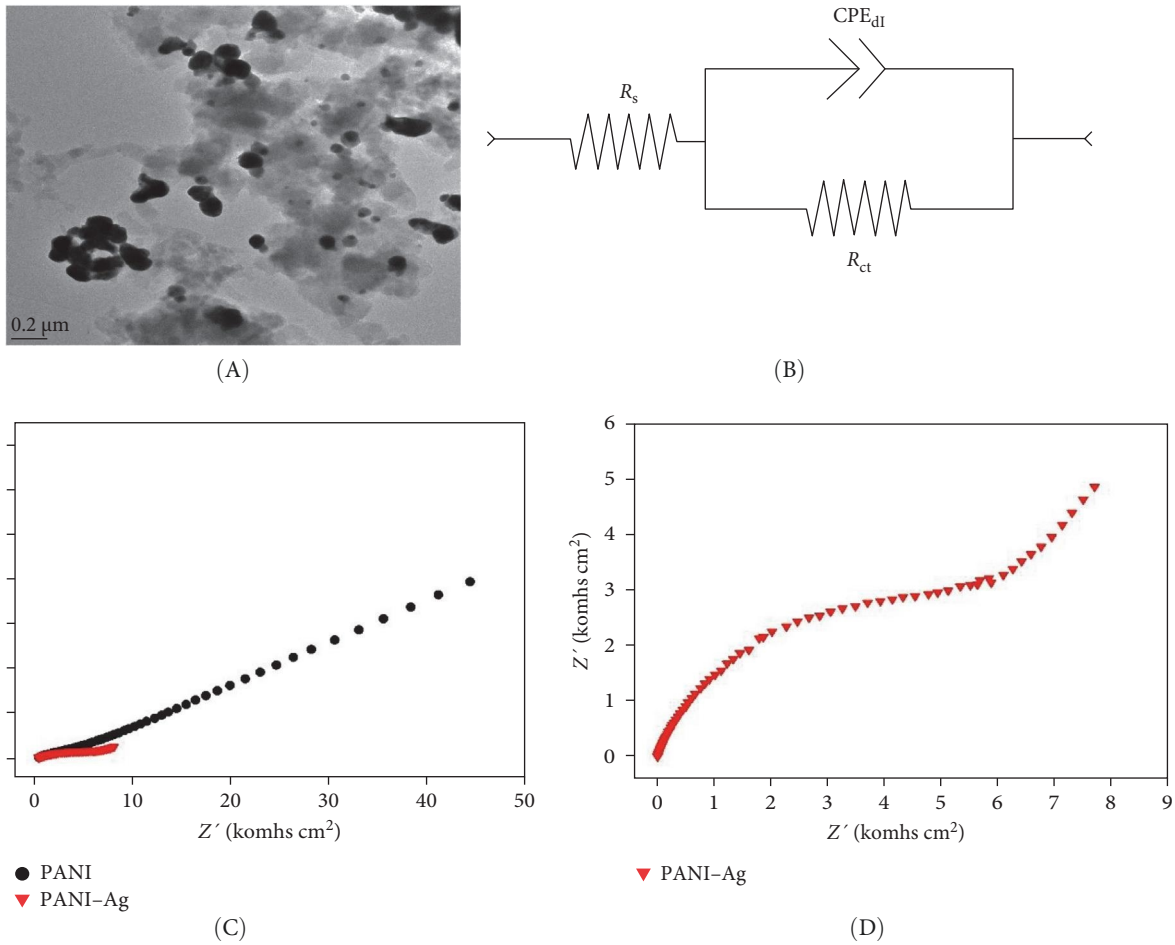

(A) (B) (C) (D)

FIGURE 3: (A) Transmission electron microscopy (TEM) images of chemically synthesized PANI–Ag (0.5 M) nanocomposite. (B) A simplified electrical equivalent circuit with R_s is the solution resistance, CPE is the constant phase element, and R_{ct} is the charge transfer. (C) Nyquist diagram for PANI, PANI–Ag (0.5 M) films at a GCE in a solution of 0.1 M HCl. (D) Nyquist diagram of PANI.

elements is due to the APS and HCl used in the PANI–Ag synthesis. The spectrum shows a significant presence of the C element, indicating that it originates from PANI. This suggests that the product is a PANI–Ag nanocomposite [49].

3.2. EIS. The parameters used for the EIS studies were the E applied (0 V), amplitude (0.01 V), frequency range (0.1–1 MHz), wave type (scan), and step type (fixed). The simplified electrical equivalent circuit in Figure 3B was used for fitting the impedance data. This equivalent circuit consists of a constant phase element (CPE), electrolyte resistance (R_s), and charge transfer resistance (R_{ct}) [50]. Figure 3C illustrates a Nyquist diagram of the EIS for PANI and PANI–Ag (0.5 M). In Figure 3C, the electron transfer or the kinetically controlled process was

9161, 2025, 1, Downloaded from https://onlinelibrary.wiley.com/doi/10.1155/js/9990501 by South African Medical Research Council, Wiley Online Library on [27/10/2026]. See the Terms and Conditions (https://onlinelibrary.wiley.com/terms-and-conditions) on Wiley Online Library for rules of use; OA articles are governed by the applicable Creative Commons License

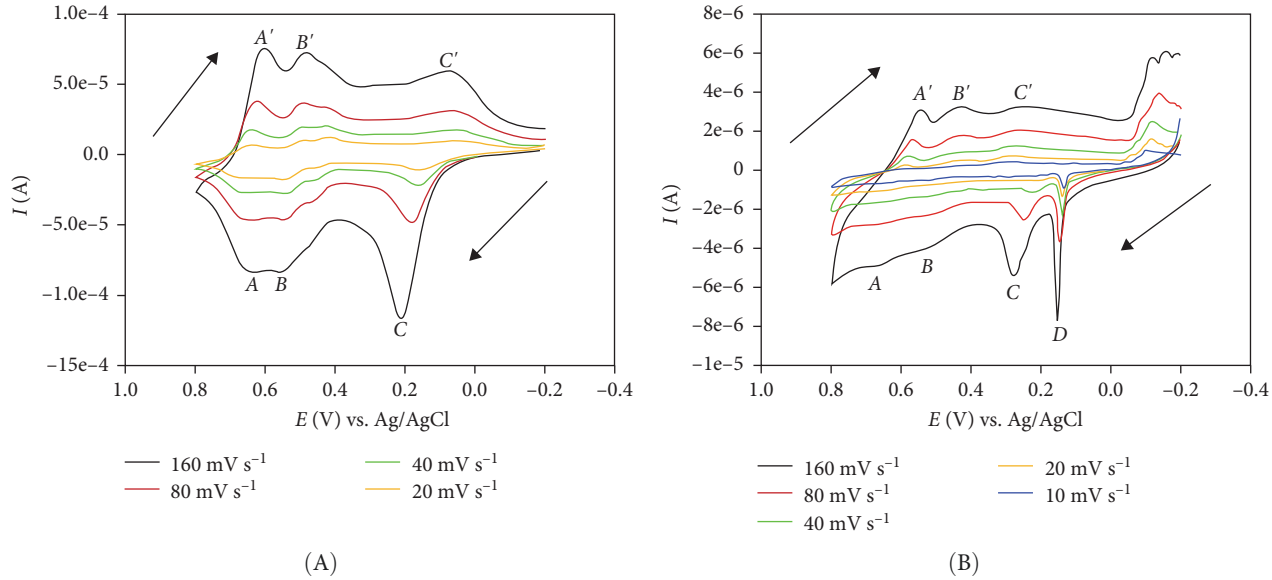

FIGURE 4: (A) CVs of chemically synthesized PANI and (B) PANI–Ag 0.5 M at a GCE in HCl solution (0.1 M). For both polymers, the potential was scanned between −0.2 and +0.8 V (vs Ag/AgCl), with scan rates ranging from 10 to 160 mV s^{-1}.

confirmed with the two plots that consist of a semicircle. According to the semicircles in Figure 3B, PANI–Ag has the smallest semicircle, which indicates that the reaction rate is the fastest in this film. The composite enhanced conductivity, increased surface area, significant electrocatalytic activity, stability, and selectivity collectively provide sufficient proof that it can effectively enhance electrocatalytic behavior in electrochemical applications, particularly in the construction of electrochemical sensors.

3.3. Cyclic Voltammetric Characterization. In the PANI study, chemical polymerization was done for the polymer preparation, followed by casting the polymer as films and dissolution in 0.1 M HCl solutions. The CV recorded for this polymer showed comparable results with the study by Somerset et al. [51] and Mathebe et al. [52] in the literature. It was observed that PANI is very soluble in an HCl solution. The electrochemical behavior for the chemically synthesized PANI was done by collecting the CV of PANI at scan rates differing from 20 to 160 mV s^{-1} using a GCE as a working electrode, with the potential scanned between −0.2 and +0.8 V (vs. Ag/AgCl). The results showed that the two prominent redox couples are generally associated with the chemically synthesized PANI. In Figure 4A, we observed redox peaks that illustrate the transformation of leucoemeraldine base to emeraldine salt and the emeraldine salt to pernigraniline salt forms (A'/A). We observed the redox peaks associated with the transformation of pernigraniline salt to emeraldine salt and emeraldine salt to the leucoemeraldine base (C'/C). The transformation of benzoquinone to hydroquinone is presented by the small redox couple obtained at +0.52 to +0.48 V (B'/B) (vs. Ag/AgCl) and can be attributed to the quinonoid rings of the PANI structure [53, 54].

Analysis of the chemically synthesized nanomaterials has shown that redox couples were illustrated in the CV results, as shown in Figure 4B for PANI–Ag (0.5 M) obtained at +0.65, +0.5, and +0.3 V (vs. Ag/AgCl) for the anodic scan and +0.55, +0.4, and +0.23 V (vs. Ag/AgCl) for the oxidation scan. The additional sharp peaks for Ag appeared along PANI redox peaks at +0.15 V and −0.02 V (vs. Ag/AgCl) [55]. These peaks are comparable to the results obtained for Ag in the study done by Paulraj et al. [56] and Bouazza et al. [42].

For the chemically synthesized polymers of PANI and PANI–Ag, the surface concentrations of these two electroactive species, the Γ^* of the two polymers, can be calculated. The Brown–Anson Equation can be used, which is a linear plot of I_p vs v. The surface concentration of the electroactive PANI–Ag (Γ^*) at the PANI–Ag/GCE sensor surface was calculated by Equation (1). In this equation, A refers to electrode area (cm^2), and Γ^* refers to the surface concentration of PANI–Ag (mole cm^{-2}). The Faraday constant refers to F, the number of electrons refers to n, R is the gas constant, the peak current refers to I_p, and T is the absolute temperature. From the straight line of the I_p vs. v curve (not shown), we calculated n to be 1.95 (2.0) for the anodic process, which illustrates that PANI–Ag undergoes a two-electron reaction at the GCE surface in 0.1 M HCl solution. The PANI–Ag surface concentration was calculated to be 9.37×10^{-10} mole cm^{-2}.

$$I_p = \frac{n^2 F^2 A \Gamma^*}{4RT} v, \tag{1}$$

$$Q = nFA\Gamma^*, \tag{2}$$

$$I_p = \frac{nFQv}{4RT}. \tag{3}$$

The electron transport diffusion coefficient, D (in cm^2 s^{-1}), for PANI–Ag was determined from Equation (4) (Randle–Sevcik equation) [57]. A straight line of I_{pc} vs. $v^{1/2}$ was constructed, and D was calculated to be 3.4×10^{-20} cm^2 s^{-1}.

9161, 2025, 1, Downloaded from https://onlinelibrary.wiley.com/doi/10.1155/js/9990501 by South African Medical Research Council, Wiley Online Library on [27/10/2026]. See the Terms and Conditions (https://onlinelibrary.wiley.com/terms-and-conditions) on Wiley Online Library for rules of use; OA articles are governed by the applicable Creative Commons License

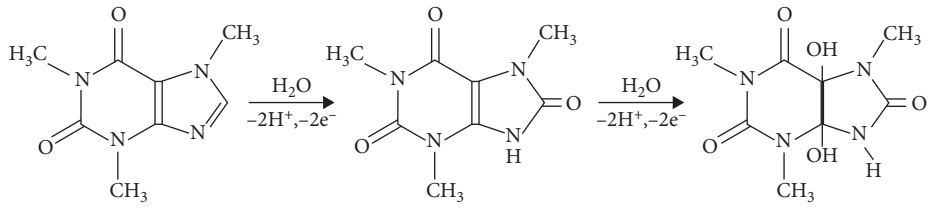

FIGURE 5: A mechanism for the electrochemical oxidation of caffeine at the sensor surface [58].

$$I_p = (2.69 \times 10^5)\, n^{3/2} D^{1/2} A C_b v^{1/2}. \quad (4)$$

Figure 5 showcases the complete CAF process that contains four protons and four electrons in several steps. In the first step, we observed two-proton and two-electron oxidation that led to the replaced uric acid (UA). The second step also illustrates a two-proton and two-electron oxidation that gives 4,5-diol analogs of methylated UA, which quickly fragments [59, 60].

3.4. Effect of Scan Rate. The voltammetric behavior in a 50 μM CAF was studied by CV using two different electrochemical sensors, such as the PANI/GCE and the PANI–Ag/GCE, in 0.1 M PBS (pH 5.0), to select the best sensor. From Figure 6A, the most significant sensor responses were obtained by the PANI–Ag/GCE sensor. The highest peak current response was obtained, making this sensor suitable for further analysis. CV was employed to explore the influence of potential scan rate on the anodic peak current of CAF at PANI–Ag/GCE (Figure 6B). The anodic peak current (I_{pa}) increases by increasing the scan rates from 20 to 160 mV s^{-1}. The anodic peak current signals in Figure 6C result in a linear equation of $I_{pa\ (A)} = 4.11 \times 10^{-7} C_{CAF}\ (\mu M) + 1.98 \times 10^{-5}$ with a regression coefficient of $R^2 = 0.9843$. These results for the CAF oxidation reaction illustrate a normal diffusion-controlled electrode process.

The values of α and n can be calculated according to Equations (5) and (6) (Laviron, 1979) [61]. The slopes were employed to extract the kinetic parameters, such as the transfer coefficients of an anodic peak and the transfer coefficients of a cathodic peak, in Figure 6B. The line segment slope equals $2.3RT/(1–\alpha)nF$ and $-2.3RT/\alpha nF$ for the anodic and cathodic peaks, with the determined values for the anodic transfer coefficients being 0.69 with an electron transfer number of 2.5.

$$E_{pa} = \frac{E^0 + 2.3\,RT}{(1-\alpha)nF \log v}, \quad (5)$$

$$E_{pc} = \frac{E^0 + 2.3\,RT}{\alpha nF \log v}. \quad (6)$$

Figure 6B illustrates the peak potentials for the anodic process, E_{pa}, as a function of the potential scan rate. We observed that from 10 to 160 mV s^{-1} scan rates, the E_p values were proportional to the logarithm of the scan rate. The value of k_s was calculated by using the following equation:

$$\log k_s = \alpha \log(1-\alpha) + (1-\alpha)\log\alpha - \log\left(\frac{RT}{nFv}\right) - \frac{(1-\alpha)\alpha nF\Delta E_p}{2.3\,RT}, \quad (7)$$

where n refers to the electron transfer number, α is the transfer coefficient of electrons, and k_s refers to the standard electron transfer rate constant. All the extracted experimental data were applied in Equation (7) to calculate the value of k_s, and it was to be 1.64 s^{-1}. The value of k_s for this study is compared with other PANI composites from the literature and tabulated in Table 1. The value of k_s for the PANI–Ag composite is the lowest compared to other composites (The Laviron plot is shown in Supporting Information 2: Figure S2).

3.5. Analytical Performance of the Coupled Method. Figure 6D compares 50 μM CAF DPV curves in PBS (pH 5.0) recorded at a PANI/GCE and PANI–Ag/GCE. The PANI–Ag/GCE showed the highest peak current responses at more positively shifted potentials when compared to the PANI/GCE. This study investigated method validation, such as LODs, correlation coefficients, and linearity. This investigation was performed in triplicate at the PANI–Ag/GCE sensor surface. DPVs curves of CAF with concentrations that increase, ranging from 10 to 90 μM, are shown in Figure 7A. Figure 7B illustrates the calibration plot of these CAF concentrations with a calibration equation of $I_p = 0.0038\,C + 0.1145$ ($R^2 = 0.9935$, $n = 3$), where the voltammetric response (I_p) is shown in μA and the CAF concentrations in μM. The LOD was calculated using this equation ($\mathrm{LOD} = \frac{3\times(\text{standard deviation of 10 blanks})}{\text{slope of the calibration curve}}$) [65]. The CAF limit of detection determined was found to be 0.38 μM. Many electrochemical sensors have been used in the literature to detect CAF using different electrochemical procedures. Table 2 compares the analytical parameters, such as linearity range, LOD, electrochemical techniques, and a series of literature data. Compared with other sensors, PANI–Ag/GCE showcases a sufficient linear range with a significantly low detection limit for determining CAF. The sensor demonstrates a robust linear response across a concentration range of 10–90 μM, showcasing its sensitivity and precision in detecting target analytes, which is beneficial for applications requiring accurate measurement in narrow concentration spans [71, 72].

3.6. Reproducibility. The reproducibility studies were also performed using five different PANI–Ag/GCE sensors for the electrochemical determination of a 50 μM concentration of CAF in a PBS (pH = 5.0) and illustrated in Figure 8. The

9161, 2025, 1, Downloaded from https://onlinelibrary.wiley.com/doi/10.1155/js/9990501 by South African Medical Research Council, Wiley Online Library on [27/10/2026]. See the Terms and Conditions (https://onlinelibrary.wiley.com/terms-and-conditions) on Wiley Online Library for rules of use; OA articles are governed by the applicable Creative Commons License

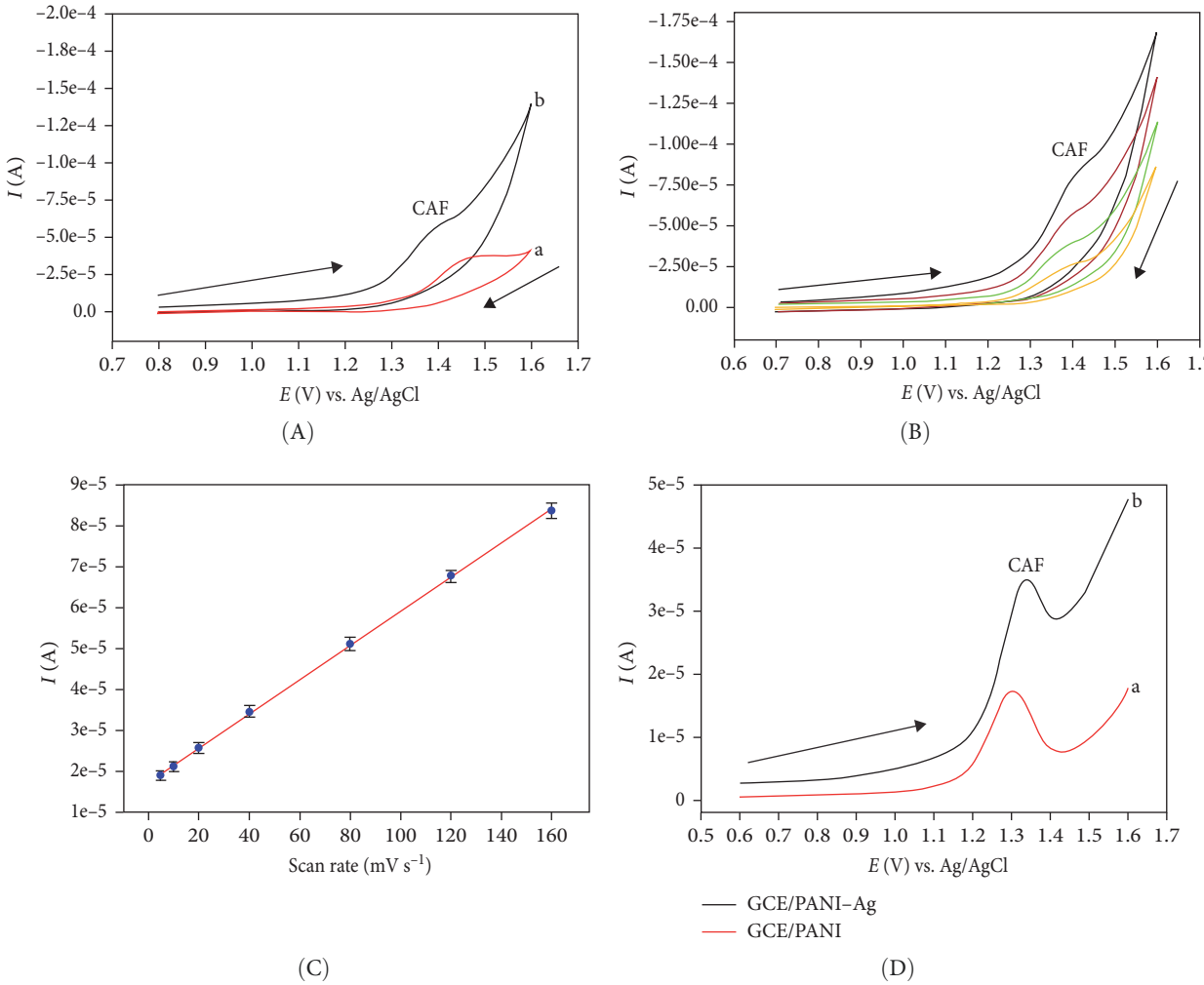

Figure 6: (A) An illustration of CVs obtained for (a) PANI/GCE and (b) PANI–Ag/GCE in 0.1 M PBS (pH = 5) containing 50 μM CAF at a scan rate of 100 mV s^{-1}. (B) The effect of scan rate studies on the CAF anodic peak current using 0.1 M PBS (pH = 5), consisting of 50 μM CAF. (C) Profile for anodic peak currents vs. scan rates. (D) DPVs were obtained for (a) PANI/GCE and (b) PANI–Ag/GCE in 0.1 M PBS (pH = 5.0) consisting of 50 μM CAF.

Table 1: Illustration of PANI–Ag/GCE sensor compared with other sensors in literature for CAF detection.

Electrode	Technique	k_s (s^{-1})	References
GOD-graphene/PANI/AuNPs-modified electrode	CV	4.8	[62]
GOx-nano-PANI/GCE	CV	6.3	[63]
Hb/PANI–TiC/GCE	CV	2.01	[64]
PANI–Ag/GCE	CV	1.64	This study

RSDs values were 3.45%–4.12% for CAF, which showcases excellent reproducibility.

3.7. Commercial Samples Analysis. The CAF concentrations were determined in commercial beverage samples, such as a carbonated soft drink and an energy drink (both from local supermarkets). The beverage samples were properly diluted before analysis to decrease the matrix effects of actual beverages. The diluting procedure was that real beverage samples of energy drinks and carbonated soft drinks were first sonicated to eliminate the gas, and then prepared a 1:10 (v/v) dilution with PBS. The experimental results are tabulated in Table 3, with the soft drink (48 mg L^{-1}) and energy drink (160 mg 500 mL^{-1}) concentrations agreeing with the declared CAF concentrations. A known amount of artificial CAF was added to the beverage samples to approve this applicability. The experimental results tabulated in Table 3 illustrate that the recoveries for CAF are within the acceptable range of 95.20%–99.65% for both soft drinks and energy drinks. Finally, the results illustrate the practical application of the developed PANI–Ag/GCE sensor to determine CAF at low levels in actual beverage samples.

9161, 2025, 1, Downloaded from https://onlinelibrary.wiley.com/doi/10.1155/js/9990501 by South African Medical Research Council, Wiley Online Library on [27/10/2026]. See the Terms and Conditions (https://onlinelibrary.wiley.com/terms-and-conditions) on Wiley Online Library for rules of use; OA articles are governed by the applicable Creative Commons License

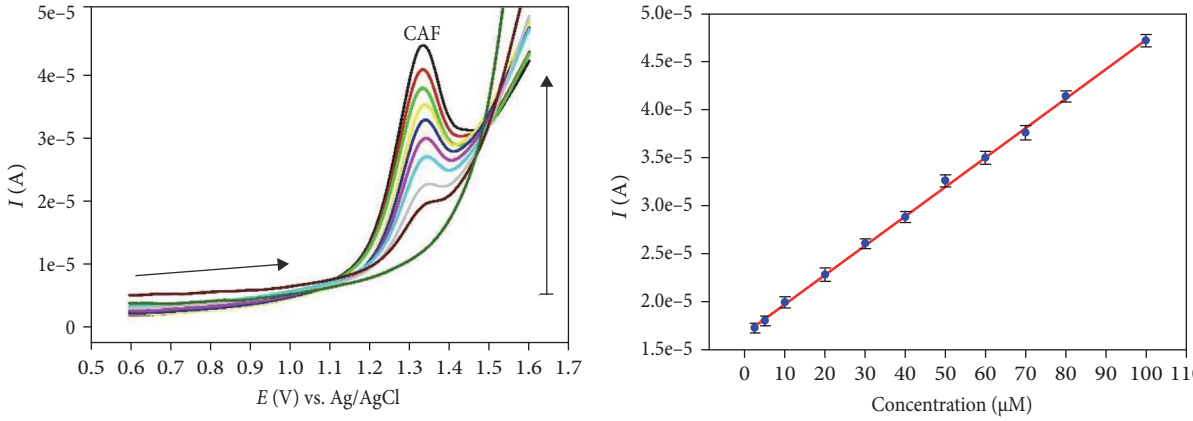

(A) (B)

Figure 7: (A) DPVs at PANI–Ag modified GCE in 0.1 M PBS (pH = 5) consist of increasing CAF concentrations 10–90 μM. (B) Calibration plot of CAF concentrations vs. anodic peak current.

Table 2: Illustration of PANI–Ag/GCE sensor compared with the linear range and detection limit of other sensors in literature for CAF detection.

Electrode	Technique	Linear range (μM)	Detection limit (μM)	References
Poly(ARS)	SWV	0.5–250	0.06	[66]
AuNP-GCPE	DPV	25–150 200–1000	0.96 4.90	[67]
m-SPME	SWV	0.5–20	0.05	[68]
GORGCPE	DPV	8–800	0.153	[69]
NCOMCP/SDS	DPV	5.0–600	0.016	[70]
AuOA-CHIT	DPV	2.0–50,000	1.00	[70]
PANI–Ag/GCE	DPV	10–90	0.38	This study

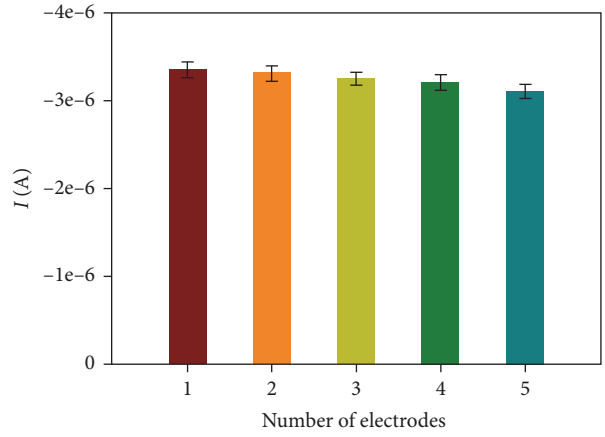

Figure 8: Reproducibility studies of the PANI–Ag/GCE using 0.1 M PBS (pH = 5) consist of 50 μM CAF.

4. Conclusions

In this study, the chemical polymerization of ANI was performed in HCl solutions. It was observed that ANI was very soluble in the HCl solution. PANI was collected as a green film on filter papers. The incorporation of Ag particles into the PANI backbone has also been performed with $AgNO_3$ aqueous solution used in the presence of APS as an oxidant. Electrochemical characterization and different spectroscopic analyses, followed by morphology characterization, were performed to study the properties of the polymer and polymer–metallic composites. Good results for the PANI incorporating Ag into the backbone of PANI were obtained. The results obtained for the morphology analysis of the composites showed that PANI and PANI–Ag are spherical. The collected results have also illustrated that the PANI–Ag

9161, 2025, 1, Downloaded from https://onlinelibrary.wiley.com/doi/10.1155/js/9990501 by South African Medical Research Council, Wiley Online Library on [27/10/2026]. See the Terms and Conditions (https://onlinelibrary.wiley.com/terms-and-conditions) on Wiley Online Library for rules of use; OA articles are governed by the applicable Creative Commons License

Table 3: Detection of CAF in a commercial carbonated energy drink and a soft drink (both from local supermarkets) samples ($n = 3$).

Sample	Spiked	Initial (mg 500 mL^{-1})	Expected (mg 500 mL^{-1})	Detected (mg 500 mL^{-1})	Recovery (%)
Carbonated soft drink	0	48	48	45.70	95.20
	10	48	58	56.90	98.10
	20	48	68	67.60	99.40
	30	48	78	77.30	99.10
Energy drink	0	160	160	155.7	97.13
	10	160	170	167.6	98.50
	20	160	180	179.4	99.65
	30	160	190	188.8	99.33

composite exhibits good electrocatalytic activity and has been employed to determine CAF in popular beverage samples. This PANI–Ag sensor was compared with other sensors in the literature. It displayed good sensitivity, wide linear concentration ranges of 10–90 μM, a low detection limit of 0.38 μM, and good reproducibility with RSD values from 3.45% to 4.12%. The PANI–Ag/GCE sensor could analyze for CAF in good agreement with the labeled values in the beverage samples.

Data Availability Statement

Data are available upon request from the authors.

Conflicts of Interest

The authors declare no conflicts of interest.

Funding

No funding was received for this manuscript.

Acknowledgments

The authors acknowledge the laboratory infrastructure and administrative support provided by the Cape Peninsula University of Technology (CPUT). The collaboration with the Universidade Federal de Goiás, Brazil, research laboratories is greatly acknowledged.

Supporting Information

Additional supporting information can be found online in the Supporting Information section.

Supporting Information 1. In the discussion of the TEM results, it is mentioned that the EDX spectrum showcases a very high content of the Ag element in the chemically synthesized nanocomposite and indicates that the sample is relatively pure. In Figure S1, the EDX results obtained for the PANI–Ag nanoparticles are showcased, and the incorporation of silver (Ag) is clearly shown.

Supporting Information 2. In the discussion of the results in Figure 6B, it is mentioned that the Epa, as a function of the potential scan rate, was evaluated. For the scan rates from 10 to 160 mV s^{-1}, the E_p values were proportional to the logarithm of the scan rate. A Laviron plot was constructed, and Equation (7) was used the evaluate the scan rate data. The Laviron plot is shown in Figure S2.

References

[1] A. C. Torres, M. M. Barsan, and C. M. Brett, "Simple Electrochemical Sensor for Caffeine Based on Carbon and Nafion-Modified Carbon Electrodes," *Food Chemistry* 149 (2014): 215–220.

[2] L. Švorc, P. Tomčík, J. Svítková, M. Rievaj, and D. Bustin, "Voltammetric Detection of Caffeine in Beverage Samples on Bare Boren-Doped Diamond Electrode," *Food Chemistry* 135, no. 3 (2012): 1198–1204.

[3] W. Y. H. Khoo, M. Pumera, and A. Bonanni, "Graphene Platforms for the Detection of Caffeine in Real Samples," *Analytica Chimica Acta* 804 (2013): 92–97.

[4] M. A. Rostagno, N. Manchón, M. D'Arrigo, et al., "Fast and Simultaneous Determination of Phenolic Compounds and Caffeine in Teas, Mate, Instant Coffee, Soft Drink and Energetic Drink by High-Performance Liquid Chromatography Using a Fused-Core Column," *Analytica Chimica Acta* 685, no. 2 (2011): 204–211.

[5] P. R. Gardinali and X. Zhao, "Trace Determination of Caffeine in Surface Water Samples by Liquid Chromatography-Atmospheric Pressure Chemical Ionization-Mass Spectrometry (LC-APCI-MS)," *Environment International* 28, no. 6 (2002): 521–528.

[6] Z. A. Al-Othman, A. Aqel, M. K. E. Alharbi, Y. A. Badjah-Hadj-Ahmed, and A. A. Al-Warthan, "Fast Chromatographic Determination of Caffeine in Food Using a Capillary Hexyl Methacrylate Monolithic Column," *Food Chemistry* 132, no. 4 (2012): 2217–2223.

[7] J. Zou and N. Li, "Simple and Environmental Friendly Procedure for the Gas Chromatographic-Mass Spectrometric Determination of Caffeine in Beverages," *Journal of Chromatography A* 1136, no. 1 (2006): 106–110.

[8] S. S. Verenitch, C. J. Lowe, and A. Mazumder, "Determination of Acidic Drugs and Caffeine in Municipal Wastewaters and Receiving Waters by Gas Chromatography-Ion Trap Tandem Mass Spectrometry," *Journal of Chromatography A* 1116, no. 1-2 (2006): 193–203.

[9] A. R. Khorrami and A. Rashidpur, "Development of a Fiber Coating Based on Molecular Sol-Gel Imprinting Technology for Selective Solid-Phase Micro Extraction of Caffeine From Human Serum and Determination by Gas Chromatography/Mass Spectrometry," *Analytica Chimica Acta* 727 (2012): 20–25.

[10] A. Belay, "Measurement of Integrated Absorption Cross-Section, Oscillator Strength and Number Density of Caffeine in

9161, 2025, 1, Downloaded from https://onlinelibrary.wiley.com/doi/10.1155/js/9990501 by South African Medical Research Council, Wiley Online Library on [27/10/2026]. See the Terms and Conditions (https://onlinelibrary.wiley.com/terms-and-conditions) on Wiley Online Library for rules of use; OA articles are governed by the applicable Creative Commons License

Coffee Beans by Integrated Absorption Coefficient Technique," *Food Chemistry* 121, no. 2 (2010): 585–590.

[11] V. R. Sinija and H. N. Mishra, "FT-NIR Spectroscopy for Caffeine Estimation in Instant Green Tea Powder and Granules," *LWT Food Science and Technology* 42 (2009): 998–1002.

[12] Z. Bouhsain, M. J. Garrigues, S. Garrigues, and M. De LaGuardia, "Flow Injection Fourier Transform Infrared Determination of Caffeine in Coffee," *Vibrational Spectroscopy* 21 (1999): 143–150.

[13] C. W. Huck, W. Guggenbichler, and K. G. Bonn, "Analysis of Caffeine, Theobromine and Theophylline in Coffee by Near Infrared Spectroscopy (NIRS) Compared to High-Performance Liquid Chromatography (HPLC) Coupled to Mass Spectrometry," *Analytica Chimica Acta* 538 (2005): 195–203.

[14] G. Del Campo, I. Berregi, R. Caracena, and J. Zuriarrain, "Quantitative Determination of Caffeine, Formic Acid, Trigonelline and 5-(hydroxymethyl) Furfural in Soluble Coffees by ^{1}H NMR Spectrometry," *Talanta* 81, no. 1-2 (2010): 367–371.

[15] M. Velmuruga, N. Karikalan, S. M. Chen, and C. Karuppiah, "Core-Shell like Cu_2O Nanocubes Enfolded With $Co(OH)_2$ on Reduced Graphene Oxide for the Amperometric Detection of Caffeine," *Microchimica Acta* 183 (2016): 2713–2721.

[16] R. Jagadish, S. Yellappa, M. Mahanthappa, and K. B. Chandrasekhar, "Zinc Oxide Nanoparticle-Modified Glassy Carbon Electrode as a Highly Sensitive Electrochemical Sensor for the Detection of Caffeine," *Journal of the Chinese Chemical Society* 64, no. 7 (2017): 813–821.

[17] Y. Zhang, J. Shang, B. Jiang, X. Zhou, and J. Wang, "Electrochemical Determination of Caffeine in Oolong Tea Based on Polyelectrolyte Functionalized Multi-Walled Carbon Nanotube," *International Journal of Electrochemical Sciences* 12, no. 3 (2017): 2552–2562.

[18] Y. Wang, Y. Ding, L. Li, and P. Hu, "Nitrogen-Doped Carbon Nanotubes Decorated Poly (L-Cysteine) as a Novel, Ultrasensitive Electrochemical Sensor for Simultaneous Determination of Theophylline and Caffeine," *Talanta* 178 (2018): 449–457.

[19] S. Chitravathi and N. Munichandraiah, "Voltammetric Determination of Paracetamol, Tramadol and Caffeine Using Poly (Nile Blue) Modified Glassy Carbon Electrode," *Journal of Electroanalytical Chemistry* 764 (2016): 93–103.

[20] Y. Wang, T. Wu, and C.-Y. Bi, "Simultaneous Determination of Acetaminophen, Theophylline and Caffeine Using a Glassy Carbon Disk Electrode Modified With a Composite Consisting of Poly (Alizarin Violet 3B), Multiwalled Carbon Nanotubes and Graphene," *Microchimica Acta* 183, no. 2 (2016): 731–739.

[21] J. Kalaiyarasi, S. Meenakshi, S. C. Gopinath, and K. Pandian, "Mediator-Free Simultaneous Determination of Acetaminophen and Caffeine Using a Glassy Carbon Electrode Modified With a Nanotubular Clay," *Microchimica Acta* 184, no. 11 (2017): 4485–4494.

[22] K. Y. Tajeu, E. Ymele, S. L. Zambou Jiokeng, and I. K. Tonle, "Electrochemical Sensor for Caffeine Based on a Glassy Carbon Electrode Modified With an Attapulgite/Nafion Film," *Electroanalysis* 31, no. 2 (2019): 350–356.

[23] D. P. Rocha, R. M. Dornellas, E. Nossol, et al., "Electrochemically Reduced Graphene Oxide for Forensic Electrochemistry: Detection of Cocaine and Its Adulterants Paracetamol, Caffeine and Levamisole," *Electroanalysis* 29, no. 11 (2017): 2418–2422.

[24] A. Yiğit, N. Alpar, Y. Yardım, M. Çelebi, and Z. Şentürk, "A Graphene-Based Electrochemical Sensor for the Individual, Selective and Simultaneous Determination of Total Chlorogenic Acids, Vanillin and Caffeine in Food and Beverage Samples," *Electroanalysis* 30, no. 9 (2018): 2011–2020.

[25] B. Silwana, C. Van der Horst, E. Iwuoha, and V. Somerset, "Inhibitive Determination of Metal Ions Using a Horseradish Peroxidase Amperometric Biosensor," in *State of the Art in Biosensors - Environmental and Medical Applications*, ed. T. Rinken, (INTECH, Croatia, 2013): 105–120.

[26] S. Biallozor and A. Kupniewska, "Conducting Polymers Electrodeposited on Active Metals," *Synthetic Metals* 155, no. 3 (2005): 443–449.

[27] N. K. Guimard, N. Gomez, and C. E. Schmidt, "Conducting Polymers in Biomedical Engineering," *Progress in Polymer Science* 32, no. 8-9 (2007): 876–921.

[28] J. Stejskal, M. Trchová, J. Kovářová, L. Brožová, and J. Prokeš, "The Reduction of Silver Nitrate With Various Polyanaline Salts to Polyanaline–Silver Composites," *Reactive and Functional Polymers* 69, no. 2 (2009): 86–90.

[29] S. Y. Park, M. S. Cho, and H. J. Choi, "Synthesis and Electrical Characteristics of Polyaniline Nanoparticles and Their Polymeric Composite," *Current Applied Physics* 4, no. 6 (2004): 581–583.

[30] A. A. Athawale and M. V. Kulkarni, "Polyaniline and Its Substituted Derivatives as Sensor for Aliphatic Alcohols," *Sensors and Actuators B: Chemical* 67, no. 1-2 (2000): 173–177.

[31] J. Gao, J. M. Sansiena, and H. L. Wang, "Chemical Vapour Driven Polyaniline Sensor/Actuators," *Synthetic Metals* 135-136 (2003): 809-810.

[32] E. W. Paul, A. J. Ricco, and M. S. Wrighton, "Resistance of Polyaniline Films as a Function of Electrochemical Potential and the Fabrication of Polyaniline-Based Microelectronic Devices," *The Journal of Physical Chemistry* 89, no. 8 (1985): 1441–1447.

[33] R. Nohria, R. K. Khillan, Y. Su, R. Dikshit, Y. Lvov, and K. Varahramyan, "Humidity Sensor Based on Ultrathin Polyaniline Film Deposited Using Layer-by-Layer Nano-Assembly," *Sensors and Actuators B: Chemical* 114, no. 1 (2006): 218–222.

[34] V. H. P. Bajpai, L. Goettler, J. H. Dong, and L. Dai, "Controlled Syntheses of Conducting Polymer Micro- and Nano-Structures for Potential Applications," *Synthetic Metals* 156, no. 5-6 (2006): 466–469.

[35] M. M. Oliveira, E. G. Castro, C. D. Canestraro, et al., "A Simple Two-Phase Route to Silver Nanoparticles/Polyaniline Structures," *The Journal of Physical Chemistry B* 110, no. 34 (2006): 17063–17069.

[36] Y.-O. Kang, S.-H. Choi, A. Gopalan, K.-P. Lee, H.-D. Kang, and Y. S. Song, "Tuning of Morphology of Ag Nanoparticles in the Ag/Polyaniline Nanocomposites Prepared by γ-Ray Irradiation," *Journal of Non-Crystalline Solids* 352, no. 5 (2006): 463–468.

[37] K. R. Reddy, K.-P. Lee, Y. Lee, and A. I. Gopalan, "Facile Synthesis of Conducting Polymer Metal Hybrid Nanocomposites by In-situ Chemical Oxidative Polymerization With Negatively Charge Metal Nanoparticles," *Materials Letters* 62, no. 12-13 (2008): 1815–1818.

[38] C. Van der Horst, B. Silwana, E. Iwuoha, and V. Somerset, "Spectroscopic and Voltammetric Analysis of Platinum Group Metals in Road Dust and Roadside Soil," *Environments* 5, no. 11 (2018): 120.

[39] B. Silwana, C. Van der Horst, E. Iwuoha, and V. Somerset, "Amperometric Determination of Cadmium, Lead, and Mercury Metal Ions Using a Novel Polymer Immobilised Horseradish Peroxidase Biosensor System," *Journal of Environmental Science and Health, Part A* 49, no. 13 (2014): 1501–1511.

9161, 2025, 1, Downloaded from https://onlinelibrary.wiley.com/doi/10.1155/js/9990501 by South African Medical Research Council, Wiley Online Library on [27/10/2026]. See the Terms and Conditions (https://onlinelibrary.wiley.com/terms-and-conditions) on Wiley Online Library for rules of use; OA articles are governed by the applicable Creative Commons License

[40] M. M. Rahman Khan, Y. K. Wee, and W. A. K. Mahmood, "Effects of CuO on the Morphology and Conducting Properties of PANI Nanofibers," *Synthetic Metals* 162, no. 13-14 (2012): 1065–1072.

[41] S. Bhadra, N. K. Singh, and D. Khastgir, "Electrochemical Synthesis of Polyaniline and Its Comparison With Chemically Synthesized Polyaniline," *Journal of Applied Polymer Sciences* 104, no. 3 (2007): 1900–1904.

[42] S. Bouazza, V. Alonzo, and D. Hauchard, "Synthesis and Characterisation of Ag Nanoparticles–Polyaniline Composite Powder Material," *Synthetic Metals* 159, no. 15-16 (2009): 1612–1619.

[43] A. Choudhury, "Polyaniline/Silver Nanocomposites: Dielectric Properties and Ethanol Vapour Sensitivity," *Sensors and Actuators B: Chemical* 138, no. 1 (2009): 318–325.

[44] J. Stejskal, I. Sapurina, M. Trchová, and E. N. Konyushenko, "Oxidation of Aniline: Polyaniline Granules, Nanotubes, and Oligoaniline Microspheres," *Macromolecules* 41, no. 10 (2008): 3530–3536.

[45] I. Sapurina and J. Stejskal, "The Mechanism of the Oxidative Polymerization of Aniline and the Formation of Supra Molecular Polyaniline Structures," *Polymer International* 57, no. 12 (2008): 1295–1325.

[46] H. H. Zhou, X. H. Ning, S. L. Li, J. H. Chen, and Y. F. Kuang, "Synthesis of Polyaniline Silver Nanocomposite Film by Unsymmetrical Square Wave Current Method," *Thin Solid Films* 510, no. 1-2 (2006): 164–168.

[47] S.-S. Chen, T.-C. Wen, and A. Gopalan, "Electrosynthesis and Characterization of a Conducting Copolymer Having S–S Links," *Synthetic Metals* 132, no. 2 (2003): 133–143.

[48] X. Li, Y. Gao, F. Liu, J. Gong, and L. Qu, "Synthesis of Polyaniline/Ag Composite Nanospheres Through UV Rays Irradiation Method," *Materials Letters* 63, no. 3-4 (2009): 467–469.

[49] N. V. Blinova, J. Stejskal, M. Trchová, I. Sapurina, and G. Ćirić-Marjanović, "The Oxidation of Aniline With Silver Nitrate to Polyaniline–Silver Composites," *Polymers* 50, no. 1 (2009): 50–56.

[50] J. H. O. Owino, O. A. Arotiba, P. G. L. Baker, A. Guiseppi-Elie, and E. I. Iwuoha, "Synthesis and Characterization of Poly (2-Hydroxyethyl Methacrylate)-Polyaniline Based Hydrogel Composites," *Reactive and Functional Polymers* 68, no. 8 (2008): 1239–1244.

[51] V. Somerset, J. Leaner, R. Mason, E. Iwuoha, and A. Morrin, "Development and Application of a Poly(2,2′-Dithiodianiline) (PDTDA)-Coated Screen-Printed Carbon Electrode in Inorganic Mercury Determination," *Electrochimica Acta* 55, no. 14 (2010): 4240–4246.

[52] N. G. R. Mathebe, A. Morrin, and E. I. Iwuoha, "Electrochemistry and Scanning Electron Microscopy of Polyaniline/Peroxidase-Based Biosensor," *Talanta* 64, no. 1 (2004): 115–120.

[53] V. Somerset, B. Silwana, C. Van der Horst, and E. Iwuoha, "Construction and Evaluation of a Carbon Paste Electrode Modified With Polyaniline-co-Poly(dithiodianiline) for Enhanced Stripping Voltammetric Determination of Metal Ions," in *Sensing in Electroanalysis*, ed. K. Kalcher, R. Metelka, I. Švancara, and K. Vytřas, (University Press Centre, 978-80-7395-782-7, 2014): 143–154.

[54] V. Somerset, E. Iwuoha, and L. Hernandez, "Stripping Voltammetric Measurement of Trace Metal Ions at Screen-Printed Carbon Paste Electrodes," *Procedia Chemistry* 1, no. 1 (2009): 1279–1282.

[55] J. Wang, J. Lu, S. B. Hocevar, P. A. M. Farias, and B. Ogorevc, "Bismuth-Coated Carbon Electrodes for Anodic Stripping Voltammetry," *Analytical Chemistry* 72, no. 14 (2000): 3218–3222.

[56] P. Paulraj, N. Janaki, S. Sandhya, and K. Pandian, "Single Pot Synthesis of Polyaniline Protected Silver Nanoparticles by Interfacial Polymerization and Study Its Application on Electrochemical Oxidation of Hydrazine," *Colloids and Surfaces A: Physicochemical and Engineering Aspects* 377, no. 1–3 (2011): 28–34.

[57] A. J. Bard and L. R. Faulkner, *Electrochemical Methods: Fundamentals and Applications* (Wiley, 2000): 978.

[58] E. Laviron, "General Expression of the Linear Potential Sweep Voltammogram in the Case of Diffusionless Electrochemical Systems," *Journal of Electroanalytical Chemistry and Interfacial Electrochemistry* 101, no. 1 (1979): 19–28.

[59] N. Alpar, Y. Yardım, and Z. Şentürk, "Selective and Simultaneous Determination of Total Chlorogenic Acids, Vanillin and Caffeine in Foods and Beverages by Adsorptive Stripping Using a Cathodically Pretreated Boron-Doped Diamond Electrode," *Sensors and Actuators B: Chemical* 257 (2018): 398–408.

[60] Y. Tadesse, A. Tadese, R. C. Saini, and R. Pal, "Cyclic Voltammetric Investigation of Caffeine at Anthraquinone Modified Carbon Paste Electrode," *International Journal of Electrochemistry* 2013 (2013): 849327.

[61] Q. Xu, S.-X. Gu, L. Jin, et al., "Graphene/Polyaniline/Gold Nanoparticles Nanocomposite for the Direct Electron Transfer of Glucose Oxidase and Glucose Biosensing," *Sensors and Actuators B: Chemical* 190 (2014): 562–569.

[62] M. Zhao, X. Wu, and C. Cai, "Polyaniline Nanofibers: Synthesis, Characterization, and Application to Direct Electron Transfer of Glucose Oxidase," *The Journal of Physical Chemistry C* 113, no. 12 (2009): 4987–4996.

[63] S. Zhang, D. Zhang, Q. Sheng, and J. Zheng, "PANI–TiC Nanocomposite Film for the Direct Electron Transfer of Hemoglobin and Its Application for Biosensing," *Journal of Solid State Electrochemitry* 18, no. 8 (2014): 2193–2200.

[64] C. Van der Horst, B. Silwana, E. Iwuoha, E. Gil, and V. Somerset, "Improved Detection of Ascorbic Acid With a Bismuth-Silver Nanosensor," *Food Analytical Methods* 9, no. 9 (2016): 2560–2566.

[65] C. Van der Horst and V. Somerset, "Nanoparticles Application in the Determination of Uric Acid, Ascorbic Acid, and Dopamine," *Russian Journal of Electrochemistry* 58, no. 5 (2022): 341–359.

[66] T. Ören and Ü. Anık, "Voltammetric Determination of Caffeine by Using Gold Nanoparticle-Glassy Carbon Paste Composite Electrode," *Measurement* 106 (2017): 26–30.

[67] H. Filik and A. A. Avan, "Conducting Polymer Modified Screen-Printed Carbon Electrode Coupled With Magnetic Solid Phase Micro Extraction for Determination of Caffeine," *Food Chemistry* 242 (2018): 301–307.

[68] M. Shehata, S. M. Azab, and A. M. Fekry, "May Glutathione and Graphene Oxide Enhance the Electrochemical Detection of Caffeine on Carbon Paste Sensor in Aqueous and Surfactant Media for Beverages Analysis?" *Synthetic Metals* 256 (2019): 116122.

[69] A. M. Fekry, M. Shehata, S. M. Azab, and A. Walcarius, "Voltammetric Detection of Caffeine in Pharmacological and Beverages Samples Based on Simple Nano-Co(II, III) Oxide Modified Carbon Paste Electrode in Aqueous and Micellar Media," *Sensors and Actuators B: Chemical* 302 (2020): 127172.

9161, 2025, 1, Downloaded from https://onlinelibrary.wiley.com/doi/10.1155/js/9990501 by South African Medical Research Council, Wiley Online Library on [27/10/2026]. See the Terms and Conditions (https://onlinelibrary.wiley.com/terms-and-conditions) on Wiley Online Library for rules of use; OA articles are governed by the applicable Creative Commons License

[70] A. Trani, R. Petrucci, G. Marrosu, D. Zane, and A. Curulli, "Selective Electrochemical Determination of Caffeine at a Gold-Chitosan Nanocomposite Sensor: May Little Change on Nanocomposites Synthesis Affect Selectivity?" *Journal of Electroanalytical Chemistry* 788 (2017): 99–106.

[71] C. Van der Horst, B. Silwana, E. Iwuoha, E. Gil, and V. Somerset, "Simultaneous Detection of Paracetamol, Ascorbic Acid, and Caffeine Using a Bismuth-Silver Nanosensor," *Electroanalysis* 32, no. 12 (2020): 3098–3107.

[72] H. Filik, A. A. Avan, and Y. Mümin, "Simultaneous Electrochemical Determination of Caffeine and Vanillin by Using Poly(Alizarin Red S) Modified Glassy Carbon Electrode," *Food Analytical Methods* 10, no. 1 (2017): 31–40.

9161, 2025, 1, Downloaded from https://onlinelibrary.wiley.com/doi/10.1155/js/9990501 by South African Medical Research Council, Wiley Online Library on [27/10/2026]. See the Terms and Conditions (https://onlinelibrary.wiley.com/terms-and-conditions) on Wiley Online Library for rules of use; OA articles are governed by the applicable Creative Commons License